International Journal of Mass Spectrometry 295 (2010) 49–59

Contents lists available at ScienceDirect

International Journal of Mass Spectrometry

journal homepage: www.elsevier.com/locate/ijms

Approximate multipole coefficients of RF ion traps as functions of aperture size

Madhurima Chattopadhyay[a], Atanu K. Mohanty[a,b,*]

[a] Department of Instrumentation, Indian Institute of Science, Bangalore 560012, India
[b] Supercomputer Education and Research Centre, Indian Institute of Science, Bangalore 560012, India

ARTICLE INFO

Article history:
Received 7 March 2010
Received in revised form 22 June 2010
Accepted 25 June 2010
Available online 16 July 2010

Keywords:
Axially symmetric (3D) ion trap
Two-dimensional (2D) ion trap
Boundary element method (BEM)
Multipole expansion coefficient

ABSTRACT

In this study we present approximate analytical expressions for estimating the variation in multipole expansion coefficients as a function of the size of the apertures in the electrodes in axially symmetric (3D) and two-dimensional (2D) ion trap ion traps. Following the approach adopted in our earlier studies which focused on the role of apertures to fields within the traps, here too, the analytical expression we develop is a sum of two terms, $A_{n,\text{noAperture}}$, the multipole expansion coefficient for a trap with no apertures and $A_{n,\text{dueToAperture}}$, the multipole expansion coefficient contributed by the aperture. $A_{n,\text{noAperture}}$ has been obtained numerically and $A_{n,\text{dueToAperture}}$ is obtained from the n th derivative of the potential within the trap.

The expressions derived have been tested on two 3D geometries and two 2D geometries. These include the quadrupole ion trap (QIT) and the cylindrical ion trap (CIT) for 3D geometries and the linear ion trap (LIT) and the rectilinear ion trap (RIT) for the 2D geometries. Multipole expansion coefficients A_2 to A_{12}, estimated by our analytical expressions, were compared with the values obtained numerically (using the boundary element method) for aperture sizes varying up to 50% of the trap dimension.

In all the plots presented, it is observed that our analytical expression for the variation of multipole expansion coefficients versus aperture size closely follows the trend of the numerical evaluations for the range of aperture sizes considered. The maximum relative percentage errors, which provide an estimate of the deviation of our values from those obtained numerically for each multipole expansion coefficient, are seen to be largely in the range of 10–15%. The leading multipole expansion coefficient, A_2, however, is seen to be estimated very well by our expressions, with most values being within 1% of the numerically determined values, with larger deviations seen for the QIT and the LIT for large aperture sizes.

1. Introduction

In this third study (after Chattopadhyay et al. [8] and Chattopadhyay and Mohanty [7]) we continue to focus our attention on apertures in the electrodes of RF ion traps. Here, we derive approximate analytical expressions for multipole expansion coefficients as a function of the size of the apertures in the electrodes. In this study, we have considered two axially symmetric (3D) and two two-dimensional (2D) ion traps.[1] The two 3D-geometry ion traps investigated include the quadrupole ion trap, QIT [18,14], and the cylindrical ion trap, CIT [12,24]. The two 2D-geometry ion traps include the linear ion trap, LIT [4], and the rectilinear ion trap, RIT [17]. In these ion traps, apertures (holes in the case of 3D and slits in the case of 2D) are machined in appropriate electrodes for the entry of electrons and the collection of destabilized fragment ions.

Multipole expansion coefficients [3] influence trap performance as well as ion dynamics in the trap. Their influence in the study of trap performance occurs on account of the appearance of the leading coefficient, A_2, in the numerator of the expression for the two Mathieu parameters a and q (e.g. [2]). These two parameters determine, for instance, voltages of ion destabilization in mass selective boundary ejection experiments [21] and the secular frequency of the ion. The influence of multipole expansion coefficients on ion dynamics can be seen in the studies of Franzen et al. [10], Sudakov [22], Abraham et al. [1] and Rajanbabu et al. [19,20]. In these studies higher order multipole expansion coefficients appearing in the governing equation of ion motion were used to understand ejection dynamics in both mass selective boundary ejection experiments as well as in resonance ejection experiments.

Currently, multipole expansion coefficients are routinely computed using numerical techniques embedded in simulation

* Corresponding author at: Supercomputer Education and Research Centre, Indian Institute of Science, Bangalore 560012, India. Tel.: +91 80 2293 2979; fax: +91 80 2360 0135.
E-mail addresses: madhuri@isu.iisc.ernet.in (M. Chattopadhyay), amohanty@serc.iisc.ernet.in (A.K. Mohanty).

[1] As pointed out in Chattopadhyay et al. [8], in this paper too the descriptor 3D refers to traps with axial symmetry, and 2D to traps with planar symmetry. It should be noted however, that the fields in both these traps are three-dimensional. In our analysis we use the symmetry to simplify the analysis and carry out a two-dimensional analysis of these traps.

1387-3806/$ – see front matter © 2010 Elsevier B.V. All rights reserved.
doi:10.1016/j.ijms.2010.06.030

packages such as ISIS [13], SPQR [16,15], ITSIM [5] and SIMION [9]. It is also easy to obtain, numerically, the variation in the multipole expansion coefficients with variation in the size of the apertures in the electrodes. What is not readily obtained in such an approach is an insight into the nature of the contribution of the aperture size in the electrodes to the multipole expansion coefficients. This insight can be provided by analytical expressions which incorporate the aperture size. The development of such analytical expressions is the motivation of the present paper.

Following the method adopted in our earlier studies [8,7], which used the theory of apertures on infinite, thin ground planes, here, too, we superpose the multipole expansion coefficients obtained in a trap with no apertures, to the multipole expansion coefficients obtained from the successive differentiation of the potential expression due to apertures. Thus, we write,

$$A_n = A_{n,\text{noAperture}} + A_{n,\text{dueToAperture}}, \tag{1}$$

where $A_{n,\text{noAperture}}$ is the n th multipole expansion coefficient in a trap with no apertures and $A_{n,\text{dueToAperture}}$ is the n th multipole expansion coefficient derived from the n th derivative of the potential or field expression due to apertures. $A_{n,\text{noAperture}}$, obtained numerically only once for a trap of a specified geometry, is the multipole expansion coefficient in a trap with no apertures in the electrodes. The expressions we present in the study are for ion traps having electrodes with finite thickness.

Although the validity of this approach has been demonstrated for the computation of on-axis and off-axis fields, the use of this approach in the context of obtaining multipole expansion coefficients needs to be tested. This is because we have used successive differentiation of the potentials for obtaining higher order multipole expansion coefficients.

We add a caveat in regard to the contents of our paper. Having obtained an analytical expression for multipole expansion coefficients, we test it against numerically obtained values and not against the fields it predicts. This is because testing for accuracy of the fields it predicts requires an entirely different exercise involving discussions, such as, the number of terms of multipole expansion coefficients that needs to be considered. This is beyond the scope of the present work. In view of this we have not undertaken any convergence studies.

In the next section, a brief description of the numerical methods used in this paper for computing the multipole expansion coefficients is provided. Section 3 presents the analytical approximation of multipole expansion coefficients with different hole radii in axially symmetric 3D traps, and Section 4 presents the expressions of multipole expansion coefficients with different slit widths in top-bottom and left-right symmetric 2D traps. The analytically estimated multipole expansion coefficients are compared with the numerically computed multipole expansion coefficients for varying the aperture dimension from 0 to 50% of the trap dimension in Section 5. Section 6 provides a few concluding remarks.

2. Numerical computations

The electrical potentials and multipole expansion coefficients for any ion trap of known geometry, can be computed numerically by using the boundary element method (BEM). The details of the BEM used in this study have already been reported in Tallapragada et al. [23] for the 3D traps and in Krishnaveni et al. [11] for the 2D traps.

In the present study, multipole expansion coefficients have been numerically computed for (1) obtaining $A_{n,\text{noAperture}}$, the multipole expansion coefficients in a trap with no apertures, and (2) for the purpose of verifying multipole expansion coefficients estimated by our theory.

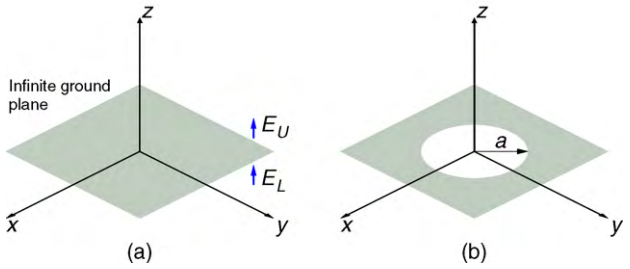

Fig. 1. (a) Schematic of an infinite thin metal plate with fields $E_L\hat{\mathbf{z}}$ and $E_U\hat{\mathbf{z}}$ on either side, $\hat{\mathbf{z}}$ being the unit vector in the z direction, and (b) the same plate with a circular hole of radius a.

3. Multipole expansion coefficients in 3D traps

3.1. Multipole expansion coefficients from the potential

In an axially symmetric ion trap, the potential U (in the spherical coordinates) can be expressed as

$$U = \Phi \sum_{n=0}^{\infty} A_n \left(\frac{r}{L}\right)^n P_n(\cos\theta). \tag{2}$$

where Φ is the applied potential difference between the ring and the endcaps. In our simulations, we have grounded the endcap electrodes and applied unit positive potential to the ring electrode. A_n are the multipole expansion coefficients, and r and θ are spherical polar coordinates. P_n represents the Legendre polynomial of the n th degree and L is the normalizing length. In our simulations, we have chosen L to be the inner waist radius r_0 of the ion trap. Due to axial symmetry, U does not depend on the ϕ coordinate. On the z-axis, $r = |z|$, $P_n(\cos\theta) = (\text{sign}\, z)^n$, and thus $U = \Phi \sum_{n=0}^{\infty} A_n z^n / L^n$. The multipole expansion coefficient, A_n, can be obtained from the n th derivative of U with respect to z, and is written as

$$A_n = \frac{L^n}{\Phi} \frac{1}{n!} \frac{\partial^n U}{\partial z^n}\bigg|_{z=0} \tag{3}$$

when the potential U is available as an analytical expression as a function of z. In our present study, we use the expression for U derived in Chattopadhyay and Mohanty [7] which has the form

$$U = U_{\text{noHole}} + U_{\text{dueToHole}}. \tag{4}$$

where U_{noHole} is the potential in the trap with no holes and $U_{\text{dueToHole}}$ is the contribution of the hole to the potential within the trap. Further, we propose that the multipole expansion coefficient of the n th degree, A_n, also be expressed in the same form as Eq. (4) as

$$A_n = A_{n,\text{noHole}} + A_{n,\text{dueToHole}}. \tag{5}$$

where $A_{n,\text{noHole}}$ is the multipole expansion coefficient in a trap with no holes in electrodes, and

$$A_{n,\text{dueToHole}} = \frac{L^n}{n!\Phi} \frac{\partial^n U_{\text{dueToHole}}}{\partial z^n}\bigg|_{z=0}, \tag{6}$$

In Eq. (5), $A_{n,\text{noHole}}$ needs to be computed numerically for the trap under investigation.

3.2. Analytical expression for multipole expansion coefficients in 3D ion traps

The contribution of a circular hole of radius a on a ground plane at $z = 0$ (as shown in Fig. 1) to the potential on the z-axis, $U_{\text{dueToHole}}$,

is given by Eq. (19) of Chattopadhyay and Mohanty [7], as

$$U_{\text{dueToHole}} = \frac{(E_U - E_L)a}{2}\left[\sigma\tau\,\text{sign}(\sigma) - \frac{2}{\pi}(\sigma\arctan\sigma + 1)\tau\right], \quad (7)$$

where E_U and E_L are the axial components of the electric field on the z-axis above and below the ground plane on the z-axis before the hole was introduced. (σ, τ, ϕ) are oblate spheroidal coordinates related to the Cartesian coordinates by

$$x = a\sqrt{(1+\sigma^2)(1-\tau^2)}\cos\phi, \quad (8)$$

$$y = a\sqrt{(1+\sigma^2)(1-\tau^2)}\sin\phi, \quad (9)$$

$$z = a\sigma\tau. \quad (10)$$

σ, τ, and ϕ have the ranges $-\infty < \sigma < \infty$, $0 \le \tau \le 1$, and $-\pi \le \phi < \pi$. It is discussed in Chattopadhyay and Mohanty [7], that on the z-axis, $\tau = 1$. Substituting $\tau = 1$ in Eq. (7) we get,

$$\begin{aligned} U_{\text{dueToHole}} &= \frac{(E_U - E_L)a}{2}\left[\sigma\,\text{sign}(\sigma) - \frac{2}{\pi}(\sigma\arctan\sigma + 1)\right] \\ &= \frac{(E_U - E_L)a}{\pi}\left[\sigma\left(\frac{\pi}{2}\,\text{sign}(\sigma) - \arctan\sigma\right) - 1\right] \\ &= \frac{(E_U - E_L)a}{\pi}\left[\sigma\arctan\frac{1}{\sigma} - 1\right] \end{aligned} \quad (11)$$

But, on the z-axis, as $\tau = 1$, using Eq. (10) we get $\sigma = z/a$. So, on the z-axis, the contribution of the hole to the potential, $U_{\text{dueToHole}}$, is given by

$$U_{\text{dueToHole}} = \frac{(E_U - E_L)a}{\pi}F_{3D}(z/a), \quad (12)$$

where,

$$F_{3D}(\zeta) = \zeta\arctan\frac{1}{\zeta} - 1 \quad (13)$$

and z/a is denoted by ζ.

For a hole at $z = z_0$, the contribution becomes

$$U_{\text{dueToHole}} = \frac{(E_U - E_L)a}{\pi}F_{3D}\left(\frac{z - z_0}{a}\right) \quad (14)$$

The contribution of a hole at $z = z_0$ to the n th multipole expansion coefficient is, therefore,

$$\begin{aligned} A_{n,\text{dueToHole}} &= \frac{L^n}{(n)!\Phi}\left.\frac{\partial^n U_{\text{dueToHole}}}{\partial z^n}\right|_{z=0} \\ &= \frac{L^n}{(n)!\Phi}\frac{E_U - E_L}{\pi a^{n-1}}F_{3D}^{(n)}\left(\frac{-z_0}{a}\right) \end{aligned} \quad (15)$$

where $F_{3D}^{(n)}$ denotes the n th derivative of F_{3D}. The method used for evaluating $F_{3D}^{(n)}$ is outlined in the next section, Section 3.3. The use of Eq. (15) for determining the n th multipole expansion coefficient in a practical trap, will now be discussed.

A trap with very thin endcaps having top-bottom symmetry is shown in Fig. 2. Due to top-bottom symmetry for both the top as well as the bottom endcaps $E_U - E_L = E_1 - E_0$. The total contribution of the two holes to the n th multipole expansion coefficient becomes

$$A_{n,\text{dueToHole}} = \frac{L^n}{(n)!\Phi}\frac{E_1 - E_0}{\pi a^{n-1}}\left[F_{3D}^{(n)}\left(\frac{-z_0}{a}\right) + F_{3D}^{(n)}\left(\frac{z_0}{a}\right)\right] \quad (16)$$

A more realistic axially symmetric trap with top-bottom symmetry is shown in Fig. 3. It has thick endcaps and bevelled holes. As discussed in Chattopadhyay et al. [8] and Chattopadhyay and Mohanty [7], a hole on a thick endcap electrode may be approximated as two separate holes on two parallel infinite thin ground planes. For the trap shown in Fig. 3, the results of four such equivalent holes on thin ground planes used to approximate the two holes on endcap electrodes, are shown in Table 1.

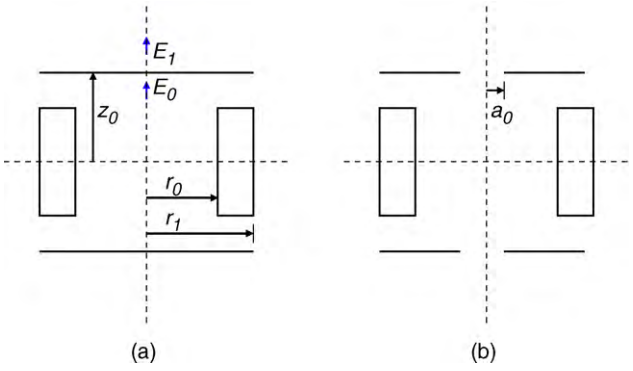

Fig. 2. Axially symmetric CIT with thin endcap electrodes. (a) Trap with no holes in the endcap electrodes and (b) the same trap with a hole of radius a_0 in the endcap electrodes.

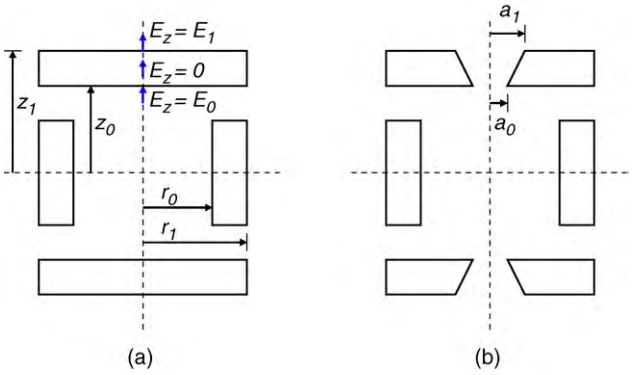

Fig. 3. Axially symmetric trap with thick endcaps. (a) Trap with no holes in the endcap electrodes and (b) the same trap with bevelled holes in the endcap electrodes.

For thick electrodes, then, $A_{n,\text{dueToHole}}$ can be written as

$$\begin{aligned} A_{n,\text{dueToHole}} = \frac{L^n}{\pi(n)!\Phi}\Bigg[&\frac{-E_0}{a_0^{n-1}}\left(F_{3D}^{(n)}\left(\frac{-z_0}{a_0}\right) + F_{3D}^{(n)}\left(\frac{z_0}{a_0}\right)\right) \\ &+ \frac{E_1}{a_1^{n-1}}\left(F_{3D}^{(n)}\left(\frac{-z_1}{a_1}\right) + F_{3D}^{(n)}\left(\frac{z_1}{a_1}\right)\right)\Bigg]. \end{aligned} \quad (17)$$

In order to obtain A_n (Eq. (5)), $A_{n,\text{dueToHole}}$ (obtained from Eq. (17)) is added to $A_{n,\text{noHole}}$ which is computed numerically.

3.3. Derivatives of F_{3D}: recurrence relations for derivatives of F_{3D}

The first three derivatives for F_{3D} are derived as

$$F'_{3D}(\zeta) = \arctan\frac{1}{\zeta} - \frac{\zeta}{1+\zeta^2}, \quad (18)$$

$$F''_{3D}(\zeta) = -\frac{2}{(1+\zeta^2)^2}, \quad (19)$$

Table 1
Locations of the planes from the centre of the trap, radii of the four holes, and field differences for the four equivalent holes corresponding to a practical trap shown in Fig. 3.

Ground plane location	Radius	Upper field E_U	Lower field E_L	$E_U - E_L$
$z = z_1$	a_1	E_1	0	E_1
$z = z_0$	a_0	0	E_0	$-E_0$
$z = -z_0$	a_0	$-E_0$	0	$-E_0$
$z = -z_1$	a_1	0	$-E_1$	E_1

and

$$F'''_{3D}(\zeta) = \frac{8\zeta}{(1+\zeta^2)^3}. \tag{20}$$

For $n \geq 2$, $F^{(n)}(\zeta)$ is of the form $\alpha_n(\zeta)/(1+\zeta^2)^n$, where α_n is a polynomial of degree $n-2$. To derive a recurrence formula for α_n we note that

$$\frac{\alpha_{n+1}(\zeta)}{(1+\zeta^2)^{n+1}} = F^{n+1}_{3D}(\zeta) = \frac{d}{d\zeta}(F^{(n)}_{3D}(\zeta))$$

$$= \frac{\alpha'_n(\zeta)}{(1+\zeta^2)^n} - 2n\zeta\frac{\alpha_n(\zeta)}{(1+\zeta^2)^{n+1}}. \tag{21}$$

Multiplying the left and right hand sides of Eq. (21) by $(1+\zeta^2)^{n+1}$ we obtain the required recurrence formula:

$$\alpha_{n+1}(\zeta) = (1+\zeta^2)\alpha'_n(\zeta) - 2n\zeta\alpha_n(\zeta) \tag{22}$$

This recurrence starts with $n=2$ for a $\alpha_2(\zeta) = -2$. No problems were encountered in the computation of derivatives up to order 12, as reported in this paper. However, no rigorous check of the stability for large n values was attempted.

4. Multipole expansion coefficients in 2D traps

4.1. Multipole expansion coefficients from potential

In a two-dimensional trap, the potential, $U(\rho, \phi)$, can be expanded in terms of multipole expansion coefficients (in the polar coordinate system) as

$$U(\rho,\phi) = \Phi\sum_{n=0}^{\infty}\left(\frac{\rho}{L}\right)^n (A_n\cos(n\phi) + B_n\sin(n\phi)). \tag{23}$$

Here Φ is the applied potential between the x-plates and the y-plates. In our simulations we have applied a potential of $-1/2$ to the pair of electrodes on the y-axis, and a potential of $+1/2$ to the other pair. ρ, ϕ are the polar coordinates. L is the normalizing length taken to be the minimum half-width between the pair of electrodes on the x-axis in our simulations. A_n, B_n are the multipole expansion coefficients. When there is top-bottom symmetry, the B_n coefficients vanish. If there is also left-right symmetry then only the even-indexed A_n survive [11]. In such a case, the potential, $U_{2D}(\rho, \phi)$, becomes

$$U_{2D}(\rho,\phi) = \Phi\sum_{k=0}^{\infty}\left(\frac{\rho}{L}\right)^{2k} (A_{2k}\cos(2k\phi)). \tag{24}$$

On the y-axis, $\rho = |y|$, and

$$\phi = \begin{cases} \pi/2 & \text{if } y > 0 \\ -\pi/2 & \text{if } y < 0 \end{cases} \tag{25}$$

Hence $\cos(2k\phi) = \cos(\pm k\pi) = (-1)^k$. Thus the potential, U_{2D}, becomes

$$U_{2D} = \Phi\sum_{k=0}^{\infty}(-1)^k\left(\frac{y}{L}\right)^{2k} A_{2k} \tag{26}$$

By following the approach given in Eq. (1), the multipole expansion coefficient A_{2k} in 2D traps can be written as

$$A_{2k} = A_{2k,\text{noSlit}} + A_{2k,\text{dueToSlit}} \tag{27}$$

In Eq. (27), the multipole expansion coefficient $A_{2k,\text{dueToSlit}}$ can be computed from the $2k$ th derivative of the potential with respect to y. $A_{2k,\text{noSlit}}$ is obtained numerically for a given trap geometry.

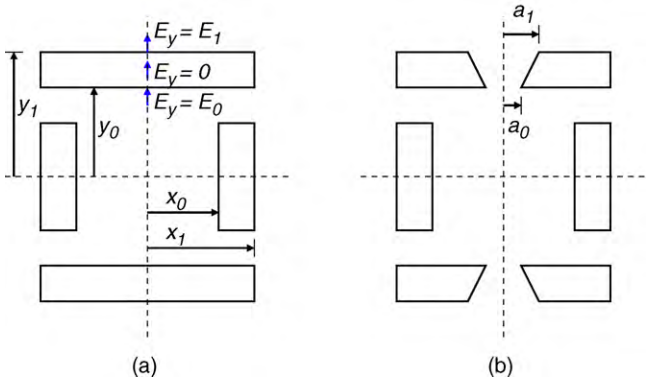

Fig. 4. 2D trap with slits in thick electrodes. (a) Trap with no slits in the electrodes and (b) Trap with bevelled slits in the electrodes.

Therefore, the even multipole expansion coefficients, $A_{2k,\text{dueToSlit}}$, can be expressed as

$$A_{2k,\text{dueToSlit}} = \frac{L^{2k}}{\Phi}\frac{(-1)^k}{(2k)!}\frac{\partial^{(2k)}U_{\text{dueToSlit}}}{\partial y^{(2k)}}\bigg|_{y=0}. \tag{28}$$

4.2. Analytical expression for multipole expansion coefficients in 2D traps

In our study, we use the analytical expression derived in Chattopadhyay and Mohanty [7] for the contribution of the slit to the potential, $U_{\text{dueToSlit}}$, which has the form

$$U_{\text{dueToSlit}} = -\frac{E_U - E_L}{2} a e^{-|\mu|}\sin\nu. \tag{29}$$

Here E_U and E_L are the y components of the electric field on the y-axis above and below the ground plane before the hole was introduced. (μ, ν) are elliptic coordinates related to the Cartesian coordinates by

$$x = a\cosh\mu\cos\nu, \tag{30}$$

$$y = a\sinh\mu\sin\nu. \tag{31}$$

Here μ and ν have the ranges $-\infty < \mu < \infty$, and $0 < \nu < \pi$, respectively. On the y-axis, $\nu = \pi/2$, and $\sinh\mu = y/a$. The term $e^{-|\mu|}\sin\nu$ in Eq. (29) then becomes $e^{-|\mu|} = \sinh|\mu| - \cosh\mu = |y/a| - \sqrt{1+(y/a)^2}$. Thus on the y-axis

$$U_{\text{dueToSlit}} = \frac{(E_U - E_L)a}{2}\left[-\left|\frac{y}{a}\right| + \sqrt{1+\left(\frac{y}{a}\right)^2}\right]$$

$$= \frac{(E_U - E_L)a}{2}F_{2D}\left(\frac{y}{a}\right), \tag{32}$$

where

$$F_{2D}(\eta) = -|\eta| + \sqrt{1+\eta^2}. \tag{33}$$

Here η is used for y/a. For a slit at $y = y_0$, Eq. (32) becomes

$$U_{\text{dueToSlit}} = \frac{E_U - E_L}{2}aF_{2D}\left(\frac{y-y_0}{a}\right) \tag{34}$$

Following the treatment in the 3D case in Fig. 4, we consider a slit on a thick electrode as a combination of two separate slits on two parallel infinite thin ground planes. As a result, four such equivalent slits on ground planes approximate the two slits in electrodes as shown by Table 2.

Table 2
Locations of the planes from the centre of the trap, half-widths, and field differences for the four equivalent slits corresponding to a practical trap shown in Fig. 4.

Ground plane location	Half-width	Upper field E_U	Lower field E_L	$E_U - E_L$
$y = y_1$	a_1	E_1	0	E_1
$y = y_0$	a_0	0	E_0	$-E_0$
$y = -y_0$	a_0	$-E_0$	0	$-E_0$
$y = -y_1$	a_1	0	$-E_1$	E_1

The contribution of the slits to the $2k$ th multipole expansion coefficient $A_{2k,\text{dueToSlit}}$, is then found to be

$$A_{2k,\text{dueToSlit}} = \frac{L^{2k}}{\Phi}\frac{(-1)^k}{2(2k)!}\left[\frac{-E_0}{a_0^{2k-1}}\left(F_{2D}^{(2k)}\left(\frac{-y_0}{a_0}\right)+F_{2D}^{(2k)}\left(\frac{y_0}{a_0}\right)\right)+\frac{E_1}{a_1^{2k-1}}\left(F_{2D}^{(2k)}\left(\frac{-y_1}{a_1}\right)+F_{2D}^{(2k)}\left(\frac{y_1}{a_1}\right)\right)\right]. \quad (35)$$

Similar to the case of the 3D traps, here too the multipole expansion coefficient A_{2k} (Eq. (27)) is obtained by summing $A_{2k,\text{noSlit}}$, which is obtained numerically, and $A_{2k,\text{dueToSlit}}$ (Eq. (35)).

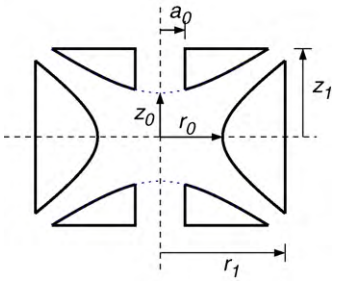

Fig. 5. Cross-sectional view of the QIT. The geometry parameters of the QIT indicated in the table are in mm.

Table 3
Maximum relative percentage errors for multipole expansion coefficients, A_2–A_{12} for the QIT.

A_2	A_4	A_6	A_8	A_{10}	A_{12}
3.58	14.47	20.27	14.85	12.67	11.43

4.3. Derivatives of F_{2D}: recurrence relations for derivatives of F_{2D}

The first three derivatives of F_{2D} are

$$F'_{2D}(\eta) = -\text{sign}(\eta) + \frac{\eta}{\sqrt{(1+\eta^2)}}, \quad (36)$$

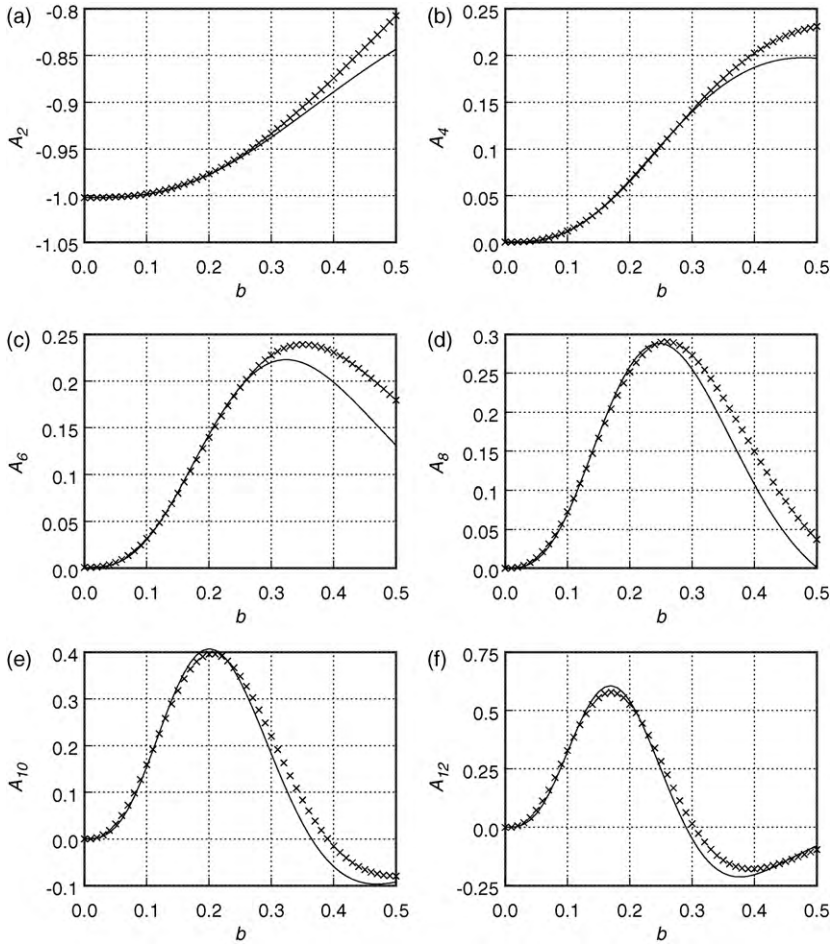

Fig. 6. Comparison between the approximated (Eq. (5)) and actual (BEM) values of multipole expansion coefficients from A_2 to A_{12} in the QIT for aperture dimension varying between 0% and 50% of trap dimension. The crosses correspond to values obtained numerically, and the continuous line corresponds to values obtained using our approximation.

Table 4
Maximum relative percentage errors for multipole expansion coefficients A_2–A_{12} for the CIT.

A_2	A_4	A_6	A_8	A_{10}	A_{12}
0.69	2.87	1.43	4.27	4.75	7.49

$$F''_{2D}(\eta) = \frac{1}{(1+\eta^2)^{3/2}}, \tag{37}$$

and

$$F'''_{2D}(\eta) = \frac{-3\eta}{(1+\eta^2)^{5/2}}. \tag{38}$$

For $n \geq 2$, $F^{(n)}_{2D}(\eta)$ is of the form $\beta_n(\eta)/(1+\eta^2)^{((2n-1)/2)}$, where β_n is a polynomial of degree $n-2$. To derive a recurrence formula for β_n we note that

$$\frac{\beta_{n+1}(\eta)}{(1+\eta^2)^{((2n+1)/2)}} = F^{(n+1)}_{2D}(\eta) = \frac{d}{d\eta}(F^{(n)}_{2D}(\eta)) = \frac{\beta'_n(\eta)}{(1+\eta^2)^{((2n-1)/2)}} - (2n-1)\eta\frac{\beta_n(\eta)}{(1+\eta^2)^{((2n+1)/2)}}. \tag{39}$$

Multiplying the left and right hand sides of Eq. (39) by $(1+\zeta^2)^{((2n+1)/2)}$ we obtain the required recurrence formula as

$$\beta_{n+1}(\eta) = (1+\eta^2)\beta'_n(\eta) - (2n-1)\eta\beta_n(\eta). \tag{40}$$

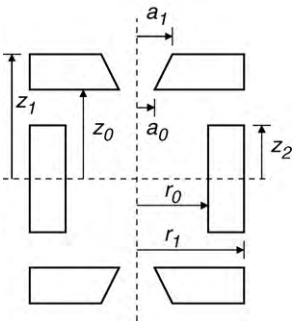

Fig. 7. Cross-sectional view of the CIT. The geometry parameters of CIT given in the table are in mm.

This recurrence starts with $n=2$ for a $\beta_2(\eta)=1$. As in the case of the 3D analysis, no problems were encountered in the computation of derivatives up to order 12. Here too, no rigorous check of the stability for large n values was attempted.

5. Results and discussion

We now turn to verifying the validity of Eqs. (5) and (27) to approximate the multipole expansion coefficients both in the 3D and the 2D ion trap geometries, respectively. In order to do this, we have chosen the QIT and the CIT to verify our expression for the 3D traps and the LIT and the RIT to verify our expression for

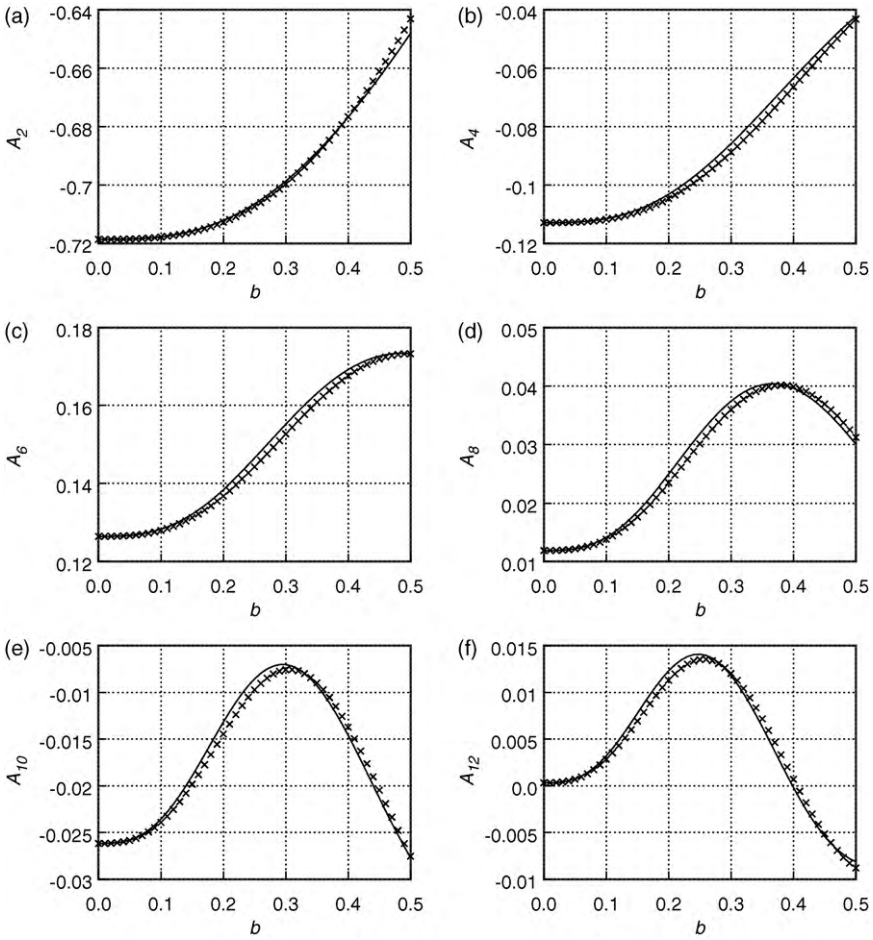

Fig. 8. Comparison between the approximated (Eq. (5)) and actual (BEM) values of multipole expansion coefficients from A_2 to A_{12} in the CIT for aperture dimension varying between 0% and 50% of trap dimension. The crosses correspond to values obtained numerically, and the continuous line corresponds to values obtained using our approximation.

the 2D traps. We will compare the estimated multipole expansion coefficients obtained using Eqs. (5) and (27) with those obtained numerically. For each of the traps considered, we have plotted even multipole expansion coefficients from A_2 to A_{12} for aperture dimensions varying from 0% to 50% of trap dimensions. We mention that such plots of multipole expansion coefficients from A_{14} to A_{24} have also been computed and presented in Chattopadhyay [6], but those have been omitted here for the sake of brevity. In each of the plots, the crosses correspond to values obtained numerically, and the continuous line corresponds to values obtained using our expression. We begin with the verification of Eq. (5) for the 3D traps and then present the results obtained using Eq. (27) for the 2D traps.

In each of the plots, we have also calculated the maximum relative percentage error, ϵ, defined by

$$\epsilon = \frac{|A_{\mathrm{BEM}} - A_{\mathrm{est}}|_{max}}{|A_{\mathrm{BEM}}|_{max}} \times 100 \tag{41}$$

where A_{BEM} is the value obtained numerically using the BEM, A_{est} is the value of the coefficient obtained by our theory and the subscript, *max*, denotes the maximum error obtained.

5.1. Axially symmetric (3D) traps

5.1.1. The QIT

Fig. 5 presents the schematic diagram of the QIT and the dimensions of the trap used in our simulations. In our simulations the ring electrode was kept at unit positive potential and the endcap electrodes were kept at ground potential.

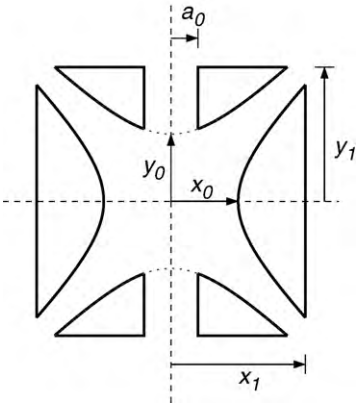

Fig. 9. Cross-section of the LIT. The geometry parameters of the LIT given in the table are in mm.

Figs. 6 presents the results for multipole expansion coefficients A_2–A_{12}, for the QIT. The values of the coefficients are indicated on the *y*-axis and the ratio, *b*, of the aperture dimension to trap dimension (waist radius of the ring electrode), a_0 / r_0, is indicated on the *x*-axis. In these computations, z_0, the distance from the centre of the trap to the endcap electrode, was recalculated for the different aperture sizes to account for the change in this distance when the aperture dimension was varied. The initial z_0 was fixed at 7.071 mm.

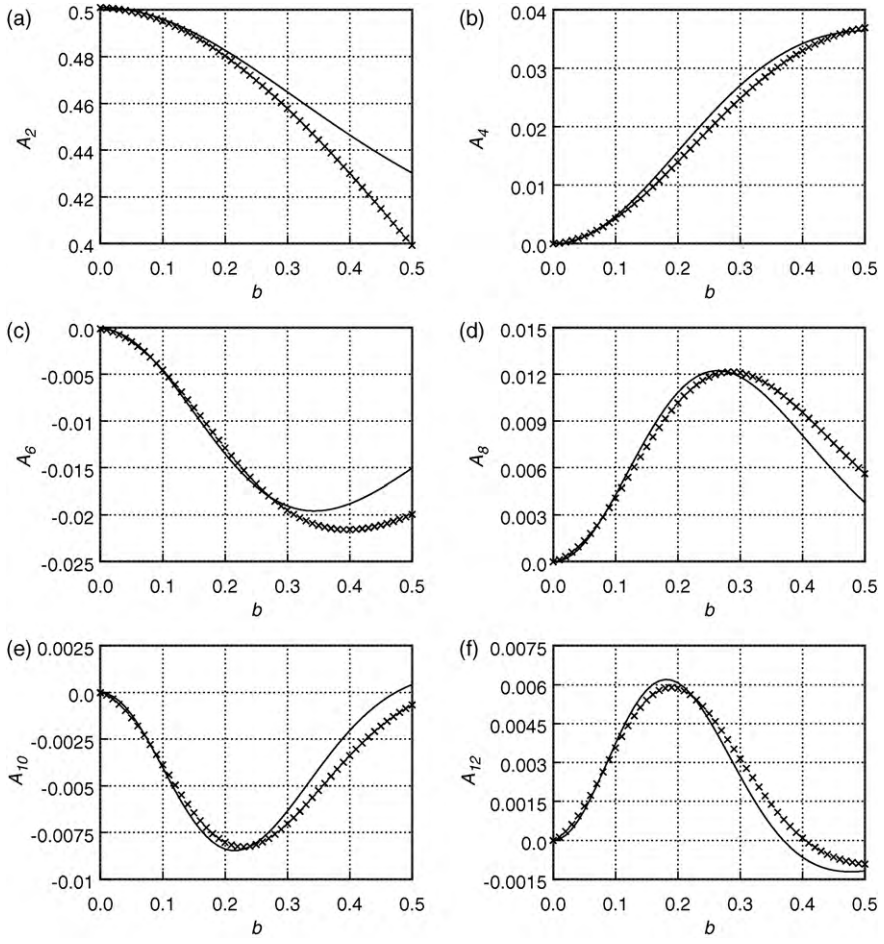

Fig. 10. Comparison between the approximated (Eq. (27)) and actual (BEM) values of multipole expansion coefficients from A_2 to A_{12} in the LIT for aperture dimension varying between 0% and 50% of trap dimension. The crosses correspond to values obtained numerically, and the continuous line corresponds to values obtained using our approximation.

Table 5
Maximum relative percentage errors for multipole expansion coefficients A_2–A_{12} for the LIT.

A_2	A_4	A_6	A_8	A_{10}	A_{12}
6.19	6.21	22.67	15.05	16.36	14.08

Table 6
Maximum relative percentage errors for multipole expansion coefficients A_2–A_{12} for the RIT.

A_2	A_4	A_6	A_8	A_{10}	A_{12}
1.75	11.91	3.35	13.04	9.92	12.69

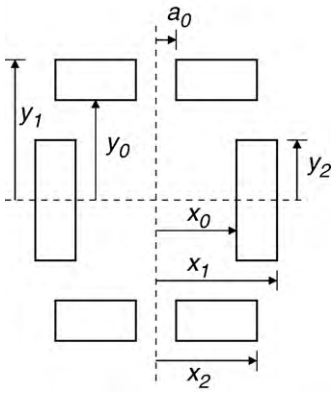

Fig. 11. Cross-sectional view of the RIT. The geometry parameters of the RIT indicated in the table are in mm.

Overall, it is seen that Eq. (5) captures the variation in the multipole expansion coefficients very well for values of b between 0 and 0.5 when compared to the numerically determined values. This is seen in all the plots, covering multipole expansion coefficients from A_2 to A_{12}. At lower values of b, the match is very close and deviations occur between the two curves only at higher values of b. A_6 has the largest calculated maximum relative percentage error of 20.27% for the value of b of 0.5. Except for A_2 where the maximum relative percentage error of 3.58% was calculated at a value of b of 0.5, all other multipole expansion coefficients have maximum relative percentage error between 10% and 16%. The maximum relative percentage errors calculated for the QIT are presented in Table 3.

5.1.2. The CIT

Fig. 7 presents the schematic diagram of the CIT geometry used in our simulations. The dimensions of the CIT geometry are given

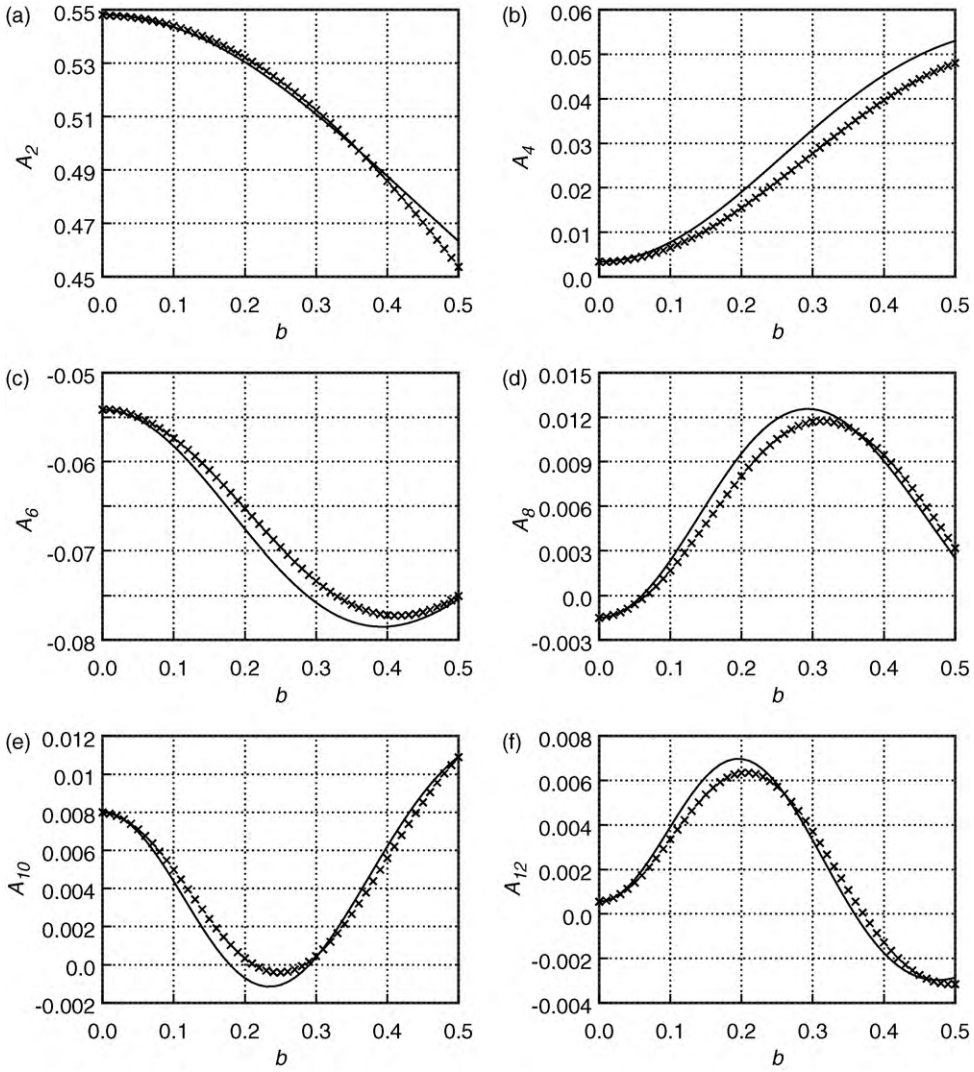

Fig. 12. Comparison between the approximated (Eq. (27)) and actual (BEM) values of multipole expansion coefficients from A_2 to A_{12} in RIT for aperture dimension varying between 0% and 50% of trap dimension. The crosses correspond to values obtained numerically, and the continuous line corresponds to values obtained using our approximation.

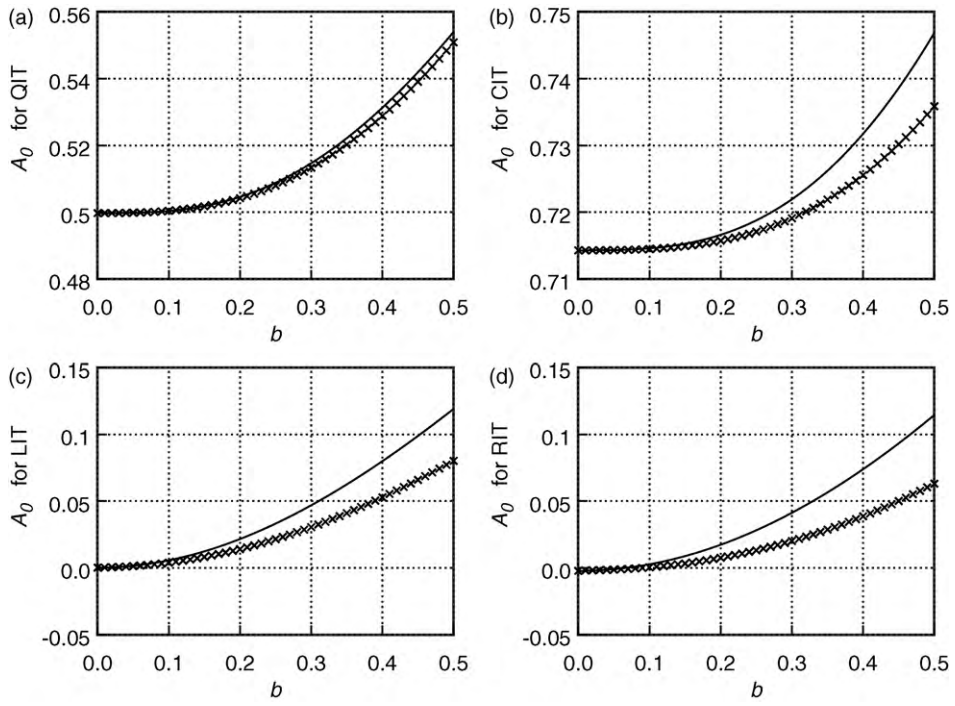

Fig. 13. Variation of A_0 for (a) the QIT of Fig. 5, (b) the CIT of Fig. 7, (c) the LIT of Fig. 9, and (d) the RIT of Fig. 11. In each subfigure the crosses indicate the values computed numerically using BEM while the continuous line indicates the values estimated using our theory.

in the table associated with the figure. All the dimensions are in mm.

For these simulations, the ring electrode was kept at unit positive potential and the endcap electrodes at ground potential. Fig. 8 presents the variation of multipole expansion coefficients A_2–A_{12}, for the CIT. The values of the coefficients are indicated on the y-axis and the ratio, b, of the aperture dimension to trap dimension (radius of the ring electrode), a_0 / r_0, is indicated on the x-axis.

As in the case of the QIT, Eq. (5) estimates the variation of multipole expansion coefficients with b very well when compared to the numerically determined values as seen in the plots A_2–A_{12}. For multipole expansion coefficients between A_2 and A_{12}, Eq. (5) estimated the coefficients for the CIT with greater accuracy than in the case of the QIT. The other multipole expansion coefficients have about the same range of maximum relative percentage errors as for the QIT. What is interesting to note is that even at a b value of 0.5, Eq. (5) and the BEM output values are close in several plots. The maximum relative percentage errors for multipole expansion coefficients are given in Table 4.

5.2. Two-dimensional (2D) traps

5.2.1. The LIT

Fig. 9 presents the schematic diagram of the linear ion trap (LIT) geometry used in our simulations. The geometry parameters are given in the table below the figure. In our simulations, one pair of electrodes (along the x-axis) was kept at a potential of +1 / 2, and the other pair of electrodes was kept at a potential of −1 / 2.

Table 7
The relative percentage errors corresponding to b for A_2.

	b					
	0.0	0.1	0.2	0.3	0.4	0.5
QIT	0.00	0.04	0.09	0.40	1.47	3.58
CIT	0.00	−0.01	−0.08	−0.14	0.02	0.69
LIT	0.00	−0.16	−0.49	−1.42	−3.28	−6.19
RIT	0.00	0.08	0.32	0.29	−0.33	−1.75

Figs. 10 presents the results for multipole expansion coefficients A_2–A_{12} for the LIT. The values of the coefficients are indicated on the y-axis and the ratio, b, of the aperture dimension to trap dimension (half-width of the trap at the waist), a_0 / x_0, is indicated on the x-axis. In these computations, y_0, the distance from the centre of the trap to the electrode in the y-axis was varied when the aperture dimension was varied to account for the change in this distance when the aperture dimension was changed. The initial y_0 was fixed at 10 mm.

Although Eq. (27) predicts the trend in the variation of multipole expansion coefficients reasonably well when compared to the values obtained using the BEM, there are deviations observed in all the plots. For the lower order multipoles (Fig. 10), there is a considerable deviation at high values of b, going up to a 22.67% deviation at A_6. Table 5 presents the relative percentage deviation for the multipole expansion coefficients.

5.2.2. The RIT

Fig. 11 presents the schematic diagram of the rectilinear ion trap (RIT) geometry used in our simulations. Its geometry parameters are specified in the table below the figure. In our simulations, one pair of electrodes (along the x-axis) was kept at a potential of +1 / 2, and the other pair of electrodes was kept at a potential of −1 / 2.

Figs. 12 present the results for multipole expansion coefficients A_2 to A_{12} for the RIT. The values of the coefficients are indicated on the y-axis and the ratio, b, of the aperture dimension to trap dimension (half-width of the trap in the x-axis), a_0 / x_0, is indicated on the x-axis.

An inspection of Fig. 12 indicates a good match between the values predicted by Eq. (27) and the BEM. The relative percentage errors for multipole expansion coefficients are given in Table 6.

5.3. Quadrupole expansion coefficient A_2

We turn to study how Eqs. (5) and (27) predict the leading multipole expansion coefficient, A_2, in comparison with the values obtained by the BEM. This has been done for different ranges

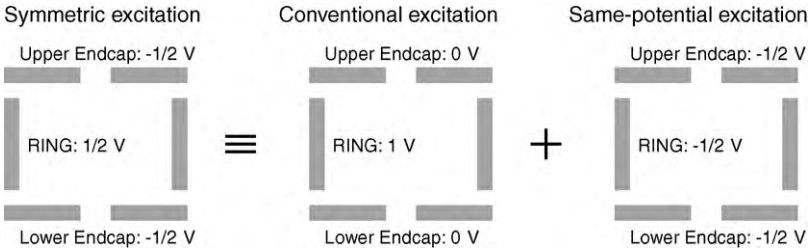

Fig. 14. The symmetric excitation of a trap can be considered as a superposition of the conventional excitation case and an excitation in which all the electrodes of the trap are at a constant potential.

Table 8
The multipole excitation coefficients for different excitations of the CIT.

Multipole expansion coefficient	Symmetric excitation	Conventional excitation	Same-potential excitation
A_0	0.21457707	0.71453932	−0.49996225
A_2	−0.71750510	−0.71754998	0.00004488
A_4	−0.11143501	−0.11138806	−0.00004695
A_6	0.12851469	0.12849740	0.00001728
A_8	0.01450078	0.01440797	0.00009281
A_{10}	−0.02319540	−0.02325915	0.00006375
A_{12}	0.00357666	0.00353402	0.00004264

of b to give an idea of how well our theory predicts the multipole expansion coefficients for different aperture sizes. Also, in order to get an idea on whether our theory under-predicts or over-predicts in comparison to the BEM, we have removed the modulus sign in Eq. (41). The results are presented in Table 7.

It is evident that our theory performs reasonably well for most cases, the exceptions being the higher values of b for the QIT and the LIT, both of which have curved-surface electrodes.

5.4. Multipole expansion coefficient A_0

Finally, we discuss the variation of the multipole expansion coefficient A_0 with aperture size. Fig. 13 shows how A_0 changes with aperture size for the four traps discussed earlier. It is seen that our theory does not predict the change in A_0 very well. This is due to the fact that the presence of the ring electrode and the truncation in the endcaps are not accounted for by our theory. It should, however, be noted that A_0 does not contribute to the field inside the trap, but is of importance when ions are transferred from one quadrupole trap to another.

5.5. Choice of potentials applied to the electrodes

In response to a query by an anonymous reviewer, we briefly consider what the multipole expansion coefficients would be if we choose the symmetric excitation of a 3D trap instead of the conventional excitation. In the symmetric excitation, the endcaps are held at a potential of $-\Phi/2$ while the ring is held at a potential of $\Phi/2$. This is in contrast to the conventional excitation where the endcaps are grounded while the ring is held at a potential of Φ.

The symmetric excitation can be considered as a superposition of the conventional excitation and a constant-potential excitation in which all the electrodes are held at $-\Phi/2$. Fig. 14 shows the three excitations for $\Phi = 1$. Since most traps are constructed in such a way that the centre of the trap is well shielded from the outside by the electrodes, the constant-potential excitation produces a very weak field inside the trap. The potential due to this excitation is nearly equal to the applied potential inside the trap. As a result, the potential inside the trap due to a constant-potential excitation only has very little of the multipole components other than the constant component A_0. We consider the CIT of Fig 7 with a hole radius of 1 mm (10% of the ring inner radius). Table 8 shows the multipole expansion coefficients for this CIT for the three types of excitations. It is seen that A_0 for the symmetric excitation is less by nearly 0.5 than the A_0 for the conventional excitation. The other multipole expansion coefficients change only marginally.

6. Concluding remarks

This study developed approximate analytical expressions for calculating multipole expansion coefficients as a function of the size of the aperture in the electrodes of axially symmetric (3D) and two-dimensional traps. These expressions for multipole expansion coefficients (Eqs. (5) and (27)) were obtained by superposing two terms, one obtained numerically for a trap with no apertures, $A_{n,\text{noAperture}}$, and the other derived from the derivatives of the potential within the trap. The expression for the potential within the trap described by Chattopadhyay and Mohanty [7] have been used in the present study.

Two 3D ion traps and the two 2D ion traps having electrodes of finite thickness have been used for verifying the utility of the expressions we have derived. The 3D traps investigated include the QIT and the CIT; the 2D traps investigated are the LIT and the RIT. The verification was done by comparing multipole expansion coefficients obtained using our expression with those obtained numerically using the BEM for the respective traps. Plots have been presented for even multipole expansion coefficients between A_2 and A_{12}, and for aperture sizes up to 50% of the characteristic dimension of the trap.

Our expression captures the trend of the variation of multipole expansion coefficients in all the traps very well, with predictions for the CIT and RIT being better than for the curved-surface electrode QIT and LIT. This is to be expected since the theory developed here used an infinite thin ground plane as its starting point. The numerical values obtained from our expression also closely match the numerically obtained value for lower aperture sizes, and a deviation is seen only at higher values of aperture size. In many cases where the relative percentage errors are large, these have to be viewed in the context of the nominal value of the multipole expansion coefficient itself being very small. Finally, it was also seen that the theory presented in this study works particularly well for the multipole A_2, which is a multipole expansion coefficient often used to study trap performance.

At this point, we feel there is scope for further improving the theory for getting a better match of multipole expansion coefficients to values obtained by the BEM. For the 3D traps, in particular, one aspect that we feel requires greater attention is the investigation of the role of the ring electrode. In some preliminary investigations, we did find that a better match was obtained when the height of ring electrode in the CIT was reduced. What this implies will require further investigations. For the 2D traps, as also for the 3D traps, we feel a limitation of our theory stems from our starting assumption that the electrodes are infinite in size. This approach may require a review. If a new theory for finite size electrodes becomes available, the approach we have adopted in this study, that of superposing multipoles expansion coefficients in traps with no apertures to coefficients contributed by the apertures, should provide a more accurate formulation.

Acknowledgement

We thank A.G. Menon and Anindya Chatterjee for discussions and suggestions on the manuscript.

References

[1] G.T. Abraham, A. Chatterjee, A.G. Menon, Escape velocity and resonant ion dynamics in Paul trap mass spectrometers, International Journal of Mass Spectrometry 231 (2004) 1–16.
[2] E.R. Badman, R.C. Johnson, W.R. Plass, R.G. Cooks, A miniature cylindrical quadrupole ion trap: simulation and experiment, Analytical Chemistry 70 (1998) 4896–4901.
[3] E. Beaty, Calculated electrostatic properties of ion traps, Physical Review A 33 (1986) 3645–3656.
[4] M.E. Bier, J.E.P. Syka, U.S. Patent 5,420,425 (1995).
[5] H.A. Bui, R. Cooks, Spectrom, International Journal of Mass Spectrometry 33 (1998) 297.
[6] M. Chattopadhyay, Ph.D. thesis, Department of Instrumentation, Indian Institute of Science, under review.
[7] M. Chattopadhyay, A.K. Mohanty, Off-axis field approximations for ion traps with apertures, International Journal of Mass Spectrometry 288 (2009) 58–67.
[8] M. Chattopadhyay, N.K. Verma, A.K. Mohanty, Composite field approximation for ion traps with apertures on electrodes, International Journal of Mass Spectrometry 282 (2009) 112–122.
[9] D.A. Dahl, SIMION for the personal computer in reflection, International Journal of Mass Spectrometry 200 (2000) 3–25.
[10] J. Franzen, R.H. Gabling, M. Shubet, Y. Wang, Nonlinear ion traps, in: R.E. March, J.F.J. Todd (Eds.), Practical Aspects of Ion Trap Mass Spectrometry, vol. 1, CRC Press, New York, 1995, p. 69.
[11] A. Krishnaveni, N.K. Verma, A.G. Menon, A.K. Mohanty, Numerical observation of preferred directionality in ion ejection from stretched rectilinear ion trap, International Journal of Mass Spectrometry 275 (2008) 11–20.
[12] D.B. Langmuir, R. Langmuir, H. Shelton, R.F. Wuerker, Containment Device, U.S. Patent 3,065,640 (1962).
[13] F.A. Londry, R.L. Alfered, R.E. March, Computer simulation of single-ion trajectories in Paul-type ion traps, Journal of the American Society for Mass Spectrometry 4 (1993) 687–705.
[14] R.E. March, R.J. Hughes, Quadrupole Storage Mass Spectrometry, Wiley–Interscience, New York, 1989.
[15] R.E. March, A.W. McMahon, E.T. Allinson, F.A. Londry, R.L. Alfred, J.F.J. Todd, F. Vedel, Resonance excitation of ions stored in a quadrupole ion trap. Part 2. Further simulation studies, International Journal of Mass Spectrometry and Ion Processes 99 (1990) 109–124.
[16] R.E. March, A.W. McMahon, F.A. Londry, R.L. Alfred, J.F.J. Todd, F. Vedel, Resonance excitation of ions stored in a quadrupole ion trap. Part 1. A simulation study, International Journal of Mass Spectrometry and Ion Processes 95 (1989) 119–156.
[17] Z. Ouyang, G. Wu, Y. Song, H. Li, W.R. Plass, R.G. Cooks, Rectilinear ion trap: concepts, calculations, and analytical performance of a new mass analyzer, Analytical Chemistry 76 (2004) 4595–4605.
[18] W. Paul, H. Steinwedel, U.S. Patent No. 2,939,952 (1960).
[19] N. Rajanbabu, A. Chatterjee, A.G. Menon, Motional coherence during resonance ejection of ions from Paul traps, International Journal of Mass Spectrometry 261 (2007) 159–169.
[20] N. Rajanbabu, A. Marathe, A. Chatterjee, A.G. Menon, Multiple scales analysis of early and delayed boundary ejection in Paul traps, International Journal of Mass Spectrometry 261 (2007) 170–182.
[21] G.C. Stafford, P.E. Kelley, J.E.P. Syka, W.E. Reynolds, J.F.J. Todd, Recent improvements in and analytical applications of advanced ion trap technology, International Journal of Mass Spectrometry 60 (1984) 85–98.
[22] M. Sudakov, Effective potential and the ion axial beat motion near the boundary of the first stable region in a non-linear ion trap, International Journal of Mass Spectrometry 206 (2001) 27–43.
[23] P.K. Tallapragada, A.K. Mohanty, A. Chatterjee, A.G. Menon, Geometry optimization of axially symmetric ion traps, International Journal of Mass Spectrometry 264 (2007) 38–52.
[24] G. Wu, R.G. Cooks, Z. Ouyang, Geometry optimization for the cylindrical ion trap: field calculations, simulations and experiments, International Journal of Mass Spectrometry 241 (2005) 119–132.